

Instabilities in an optical black-hole laser

Juan D Rincon-Estrada and David Bermudez*

Departamento de Física, Cinvestav, A.P. 14-740, 07000 Ciudad de México, Mexico

(Dated: April 7, 2022)

We study the Hamiltonian of optical fields in a nonlinear dispersive fiber. Quantum field fluctuations are created spontaneously close to an optical event horizon through the analog Hawking effect. We consider the simplest model for an optical black-hole laser, where the Hawking radiation is produced and amplified inside a cavity created by two close horizons: a black hole and a white hole. We find that the resonant Hawking radiation originates from a discrete set of instabilities and can tunnel out of the horizons. Unlike other methods, we determine the most efficiently amplified instability that dominates the resonant Hawking process.

PhySH: quantum aspects of black holes, laboratory studies of gravity, optical fibers, Kerr effect.

I. INTRODUCTION

Hawking radiation is the flux of particles with thermal spectrum that escape from a black hole [1]. It is considered a fundamental phenomenon of quantum field theory in curved spacetimes and used as a test for possible theories of quantum gravity [2, 3]. Although its formulation is based in widely accepted physical principles, its astrophysical observation seems unlikely, at least in the near future.

In 1981, Unruh realized that the same effect occurs in moving fluids [4]. This opened the possibility of observing analog Hawking radiation in the laboratory instead of directly from an astrophysical black hole. The analog phenomenon occurs close to a sonic horizon in a moving fluid—close to the interface that separates a subsonic and a supersonic current. A thermal flux of phonons is generated spontaneously from the sonic horizon into the subsonic region. This effect originates from the impossibility of defining a global vacuum state that is adapted to both fluid regions.

Unruh’s work inspired other proposals to test predictions of gravitation and cosmology with analog systems in laboratories of condensed matter and optics such as: water tanks [5, 6], liquid helium [7, 8], Bose-Einstein condensates (BECs) [9–11], optical fibers [12, 13], and spintronic materials [14]. A new configuration emerging from these studies is the so-called “black-hole laser” [15], that consists in a stationary finite transonic fluid: its flow changes from subsonic to supersonic and after a finite region back to subsonic. This establishes two horizons—one black hole (BH) and one white hole (WH)—that confine Hawking radiation in the region between them. The radiation is self-amplified because the two horizons behave as mirrors in a resonant cavity—similar to a laser. This process exists in sonic analogs (as BECs) if the quantum field is bosonic and the dispersion relation is anomalous. The same effect was extended to the optical

case to obtain an “optical black-hole laser” (OBHL) for a bosonic field and a normal dispersion relation [16, 17].

The theory of instabilities describes this amplification process [18, 19] by analyzing the quantum excitations generated spontaneously in a moving medium. This method was previously applied in condensed matter [10] and in this work we develop it in optics. We use the flat velocity profile approximation and obtain information that is usually hidden in the technical difficulties of more complicated models: Hawking radiation escapes from the cavity, the resonant modes come from a discrete set of instabilities in the system, and the cavity modes have different lifetimes.

This work is organized as follows. In Section II we start from the Hamiltonian for light in an optical fiber to find the dynamical equation for a quantum field and the dispersion relation for a spontaneous fluctuation. In Section III, we analyze the OBHL configuration with real frequencies and describe its kinetics. We obtain the instabilities by introducing complex frequencies in Section IV. In Section V, we compare these results with the resonances from a plane-wave model and introduce a phenomenological model to expand the physical picture. Finally, we present our conclusions in Section VI.

II. QUANTUM FLUCTUATIONS PROPAGATING IN AN OPTICAL FIBER

When an electromagnetic wave travels inside a medium, it interacts with its bound electrons, such that its group velocity depends in the optical frequency of the wave ω , as described by the material dispersion. If the medium is an optical fiber, we also consider the nonlinear coupling between the electromagnetic field of the ingoing wave and the electron polarization. Our goal is to analyze the dynamics of a quantum field fluctuation propagating inside an optical fiber and generated close to an optical horizon through the analog Hawking effect.

Let us start from the Hamiltonian for light in optical fibers by Drummond [20, 21] given by $H = H_L + H_{NL}$,

* E-mail: dbermudez@fis.cinvestav.mx;

Website: <https://www.fis.cinvestav.mx/~dbermudez/>

where H_L is the linear part of the Hamiltonian

$$H_L = \hbar \int \left[\omega \Psi^\dagger \Psi + \frac{i}{2} u (\partial_x \Psi^\dagger \Psi - \Psi^\dagger \partial_x \Psi) - \frac{1}{2} u^3 \beta_2 \partial_x \Psi^\dagger \partial_x \Psi \right] dx, \quad (1)$$

and H_{NL} is the nonlinear part

$$H_{NL} = \kappa \int \Psi^{2\dagger} \Psi^2 dx. \quad (2)$$

The excitations of the quantum field $\Psi(x, t)$ propagate inside an optical fiber and satisfy the following commutation relation

$$[\Psi(x, t), \Psi(x', t)] = \delta(x - x'). \quad (3)$$

Considering the Hamiltonian in the interaction picture, this quantum field obeys the following equation of motion

$$(\partial_t + u \partial_x) \Psi = \left[-\frac{i}{2} u^3 \beta_2 \partial_x^2 + i \kappa \Psi^\dagger \Psi \right] \Psi, \quad (4)$$

where $u = \beta_1^{-1} = (\partial_\omega \beta)^{-1}|_{\omega_c}$ is the group velocity of the field, $\beta_2 = \partial_\omega^2 \beta|_{\omega_c}$, β_2 is the group-velocity dispersion (GVD) parameter, ω_c is the central frequency, and κ is a constant that characterizes the nonlinear coupling of the field with itself. The first term in Eq. (4) suggests the following coordinate transformation

$$\tau = t - \frac{x}{u}, \quad x' = x, \quad (5)$$

that introduces a reference frame moving with the pulse. The change of coordinates also produces

$$\partial_x = \partial_{x'} - \frac{1}{u} \partial_\tau, \quad \partial_t = \partial_\tau. \quad (6)$$

Substituting Eqs. (6) in (4) and considering that $x \gg ut$, the spatial derivative can be neglected to find

$$i \partial_{x'} \Psi - \frac{\beta_2}{2} \partial_\tau^2 \Psi + \kappa \beta_1 \Psi^\dagger \Psi \Psi = 0. \quad (7)$$

This is a nonlinear Schrödinger equation (NLSE) where the time and space variables have been interchanged; this equation describes the propagation of a quantum field in a nonlinear medium ($\Psi^\dagger \Psi \Psi$) with dispersive effects ($\partial_\tau^2 \Psi$).

A. Linearization of the quantum fluctuation

Consider a field propagating inside an optical fiber described by Eq. (7). If this field is a continuous wave—called pump pulse—its amplitude $\Psi(x, \tau)$ does not depend on τ as the field is stationary during propagation and we can propose

$$\Psi(x) = \sqrt{n} e^{i \kappa \beta_1 n x}, \quad (8)$$

where $n = |\Psi|^2$ is the photon density. Let us see if this solution is stable under a small fluctuation $\phi(x, \tau)$, i.e., $\Psi \rightarrow \Psi' = \Psi + \phi(x, \tau) e^{i \kappa \beta_1 n x}$ such that

$$\Psi'(x, \tau) = e^{i \kappa \beta_1 n x} [\sqrt{n} + \phi(x, \tau)]. \quad (9)$$

Inserting Eq. (9) in (7), we find the equation for the propagation of a linear fluctuation ϕ under a background field:

$$i \partial_x \phi - \frac{\beta_2}{2} \partial_\tau^2 \phi + \kappa \beta_1 n (\phi + \phi^*) = 0. \quad (10)$$

We propose a plane-wave solution

$$\phi(x, \tau) = a_1 e^{i(\beta x - \omega \tau)} + a_2^* e^{-i(\beta x - \omega \tau)}, \quad (11)$$

and separate linearly independent terms to obtain the following system of equations

$$\begin{pmatrix} -\beta + \frac{\beta_2}{2} \omega^2 + \kappa \beta_1 n & \kappa \beta_1 n \\ \kappa \beta_1 n & \beta + \frac{\beta_2}{2} \omega^2 + \kappa \beta_1 n \end{pmatrix} \begin{pmatrix} a_1 \\ a_2 \end{pmatrix} = \begin{pmatrix} 0 \\ 0 \end{pmatrix}. \quad (12)$$

The terms out of the diagonal mix positive and negative frequency (or norm) modes—an essential ingredient of the Hawking process [22]. This leads to non trivial solutions if

$$\beta^2 = \kappa n \beta_1 \beta_2 \omega^2 + \frac{\beta_2^2}{4} \omega^4, \quad (13)$$

that can be modeled as

$$\beta^2 = \frac{\omega^2}{c^2} (b_1^2 + b_2 \omega^2), \quad (14)$$

with $b_1^2 = \kappa n c^2 \beta_1 \beta_2$ and $b_2 = c^2 \beta_2^2 / 4$ given by material constants and the group velocity of the pulse. This is a normal dispersion, because $\beta(\omega)$ increases with ω as is usual in optics [17].

It is useful to replace the propagation distance x for a propagation time $\zeta = x/u$ and keep the delay as $\tau = t - x/u$ such that the frame comoving with the pulse is described by the coordinates (ζ, τ) and the comoving frequency ω' is conserved [22, 23]. The Doppler shift between the frequencies in the two frames is

$$\omega' = \gamma(\omega - u \beta_{\text{eff}}(\omega)) = \gamma \omega \left(1 - \frac{n(\omega) + \delta n}{n_{g0}} \right), \quad (15)$$

where $\gamma = (1 - u^2/c^2)^{-1/2}$, $n_{g0} = c/u$, and we used the relation $\beta_{\text{eff}}(\omega) = n_{\text{eff}}(\omega)\omega/c$. The effective refractive index $n_{\text{eff}}(\omega) = n(\omega) + \delta n$, has two contributions: the refractive index of the fiber $n(\omega)$ and the change in refractive index due to the optical Kerr effect δn . By reorganizing Eq. (15), we find the following dispersion relation

$$\left[\frac{n_{g0}}{\gamma b_1} \omega' - \omega v(\tau) \right]^2 = \omega^2 + \frac{\omega^4}{\Omega_0^2}, \quad (16)$$

where $\Omega_0^2 = b_1^2/b_2$, and we define the velocity profile of the optical medium as

$$v(\tau) = \frac{n_{g0} - \delta n(\tau)}{b_1}, \quad (17)$$

i.e., the change of the group index scaled by b_1 . We refer to this dimensionless quantity as velocity in analogy with the dispersion relation in fluids [15]. The system is stationary in the comoving medium and the change in velocity is due to the change in refractive index δn .

To simplify the notation, without loss of generality we set $b_1 = 1$ and absorb the constant n_{g0}/γ in ω' . Then, the dispersion relation for the optical case is

$$[\omega' - \omega v(\tau)]^2 = \omega^2 + \frac{\omega^4}{\Omega_0^2}. \quad (18)$$

As the dispersion relation is of forth-order in ω , a general solution for a fluctuation in the system with fixed ω' is

$$\phi(\zeta, \tau) = e^{-i\omega'\zeta} \sum_{j=1}^4 A_j e^{-i\omega_j \tau}. \quad (19)$$

B. Optical analog of the event horizon

In fluid analogs of the event horizon, the moving medium represents the black-hole spacetime and waves in the medium represent light waves. In optics, the analogy goes one step further: waves are indeed light waves, but a light pulse propagating in a dielectric replaces the moving medium or the black-hole spacetime [23].

To create an optical horizon we send a short laser pulse with optical power $I(\tau)$ —called pump—that slows down waves by raising the local refractive index of a medium by the Kerr effect:

$$n_{\text{eff}}(\omega, \tau) = n(\omega) + \delta n(\tau) = n(\omega) + n_2 I(\tau). \quad (20)$$

The resulting refractive index profile establishes the effective spacetime curvature where waves propagate. If light is slowed below the pump speed, the pump moves superluminally and two horizons are formed at the boundaries between sub- and superluminal propagation: light cannot enter the trailing edge of the pulse or cannot escape from the leading edge of the pulse. In analogy with the metric of spacetime in the vicinity of a black hole, the leading and trailing edges of the pulse act as a black hole (BH) or a white hole (WH) event horizon, respectively [12, 24]. We show the horizons created by a soliton in Fig. 1(a).

The Hawking effect is the spontaneous creation of particles around a black-hole horizon due to the mixing of positive and negative frequency modes. In the optical analog, the field is the electromagnetic field and the horizon is formed by light in a dielectric. The studies of analog systems has given us more freedom to study the Hawking effect in different configurations that cannot be obtained in astrophysics, such as the black-hole laser.

III. OPTICAL BLACK-HOLE LASER

In an optical black-hole laser (OBHL) a fluctuation generated by the analog Hawking effect is trapped and

amplified in a cavity made by light. This concept inspired the so-called temporal waveguide, where light is trapped, not in space as in a waveguide, but in time between two pulses. The temporal waveguide has been proposed as a way of increasing the data speed transmission through optical fibers [25].

The optical cavity is created in the region between two independent pumps or solitons at the same frequency ω_c and placed at a certain distance x_c (or time τ_c) from each other, such that in the comoving frame their location remains constant. Each pulse has a BH and a WH, but the cavity is formed only by the inner horizons of the two pulses [12, 17], as shown in Fig. 1(a): The cavity is the shaded region between a WH and a BH.

In a dispersive system the group velocity depends on the frequency and each frequency experiences the horizon in a different spatial point: the horizon is “fuzzy”; this complicates its theoretical analysis. For this reason we use a simplified model, where the cavity is formed, not by solitons, but by sharp changes of refractive index, called step-index model [26] or front-induced [24]. In this model, the cavity is a region with $\delta n = 0$ and the exterior with $\delta n = \delta n_{\text{max}}$ (see Fig. 1(b)).

The main difference between the soliton and the step-index model is how fast the refractive index changes. In the step-index model, the refractive index is constant and its change is discontinuous. Although both models fulfill the definition of an OBHL, the step-index is simpler and is the one we use for the theoretical studies in this work. The horizons still create analog Hawking radiation inside and outside the cavity and the cavity amplifies the trapped modes.

A. Numerical method: OBHL with real frequencies

The step-index model defines two different regions for $v(\tau)$: a subluminal region outside the cavity (I and III) where $v_1 = n_{g0} - \delta n_{\text{max}}$ and a superluminal region that forms the cavity (II) where $v_2 = n_{g0}$. Notice that $v(\tau)$ is positive because in the comoving frame the medium moves to the right. In the optical case we can only vary the velocity outside the region v_1 , while v_2 is kept fixed, unlike the sonic case, where the flow in any region can be modified [27]. This is because the velocity profile in the optical case is modified by a δn that can only decrease the effective refractive index.

The OBHL configuration is only valid for values of ω' close to the horizon ω'_h and limited by δn_{max} , see Section III C. The dispersion relation (18) is shown in Fig. 2(a), the shadowed region marks the region of comoving frequencies ($\omega'_{h-\text{max}}, \omega'_h$) trapped by the cavity.

If a fluctuation is spontaneously generated in the cavity with frequency $\omega_{2\text{ur}}$, its comoving frequency $\omega'(\omega_{2\text{ur}})$ would be conserved. This mode can be dispersed into four possible modes in the cavity and two outside. These modes are shown in Fig. 2(a) and are obtained by numerically solving Eq. (18) for v_1 and v_2 .

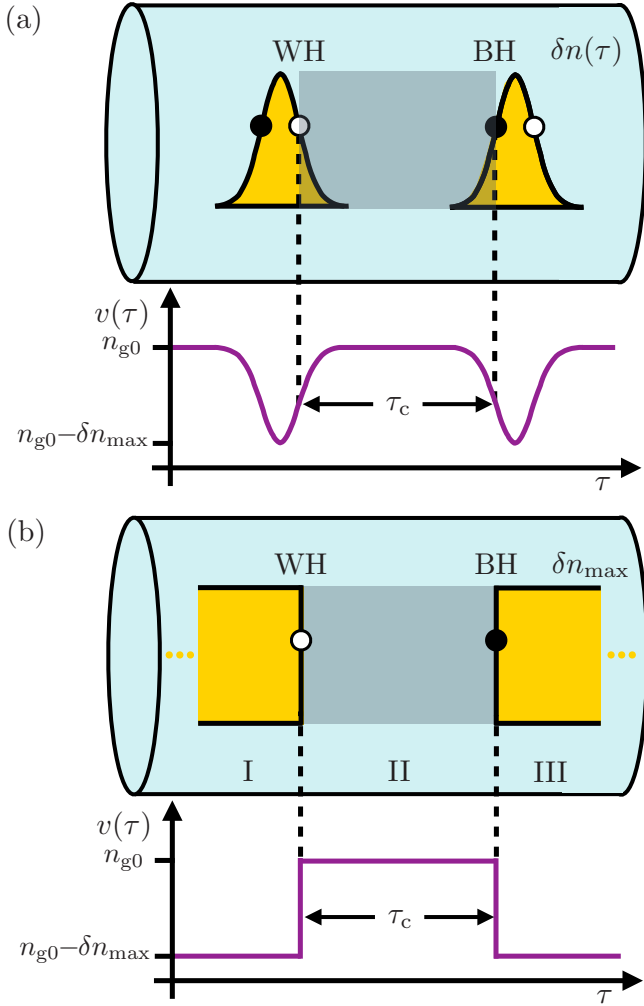


FIG. 1. (a) Cavity formed by two solitons in the comoving frame, where the white- (WH) and black- (BH) hole horizons are marked. (b) Cavity in the step index model. Below each image we show the corresponding velocity profile $v(\tau)$, marking three regions: I and III are the subluminal regions or exterior, and II is the superluminal region or cavity.

The frequency modes that solve Eq. (18) are labeled with a subindex ‘u’ for counterpropagating or ‘v’ for copropagating modes and ‘1’ for those in the subluminal region v_1 or ‘2’ in the superluminal one v_2 . In Fig. 2(a), the copropagating branch for the relevant frequencies is almost a straight line, reflecting that these modes are not dispersed, while the counterpropagating branch is a highly dispersive curve. For $\omega < 0$, the solutions labeled as ω_{1u} and ω_{2u} are negative-frequency or negative-norm modes [28]. For $\omega > 0$ and v_1 there is only one solution in the copropagating branch ω_{1v} , for v_2 there are three modes, one copropagating ω_{2v} and two counterpropagating ω_{2ul} and ω_{2ur} . The labels in the last two solutions specify if the modes move to the left (l) or right (r) in the comoving frame. Modes ω_{2ul} and ω_{2ur} can be confined in the cavity [27], as they fulfill the resonance condition,

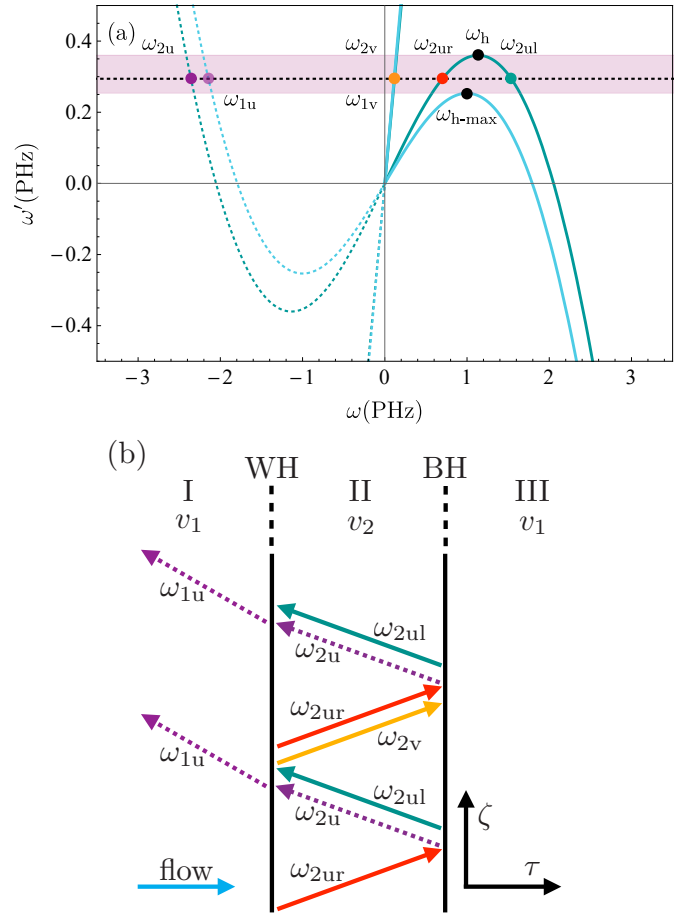


FIG. 2. (a) Dispersion relation (18) in the comoving frame for the subluminal regions with δn_{\max} (blue) and for the superluminal region with $\delta n = 0$ (green). The colored stripe marks the interval of comoving frequencies for the OBHL configuration. The conservation of comoving frequency gives two modes ω_{1u} and ω_{1v} in the subluminal regions and four ω_{2u} , ω_{2v} , ω_{2ur} , and ω_{2ul} in the superluminal region. The parameters are $\omega' = 0.294\text{PHz}$, $\Omega_0 = 1.861\text{PHz}$, $n_{g0} = 1.488$, and $\delta n_{\max} = 0.1$. (b) Diagram of the evolution of a trapped mode ω_{2ur} for real frequencies, the escaping mode ω_{1u} is the resonant Hawking radiation. Solid [dashed] lines refer to positive [negative] frequency modes.

see Fig. 2(b) and Section V.

B. Direction of travel

The direction of travel is given by the sign of the group velocity v_g for the frequency modes of dispersion relation (18):

$$v_g(\omega, \delta n) = \frac{\partial \omega}{\partial \beta} = \frac{c}{\delta n + \frac{2\omega^2 + \Omega_0^2}{\omega^2 + \Omega_0^2} \sqrt{1 + \frac{\omega^2}{\Omega_0^2}}}. \quad (21)$$

The counterpropagating modes (u) move with positive velocity (to the right in the laboratory frame) and the copropagating modes (v) move with negative velocity

$$v_u(\omega, \delta n) = v_g(\omega, \delta n), \quad v_v(\omega, \delta n) = -v_g(\omega, \delta n). \quad (22)$$

We can describe the modes in the subluminal region with $\delta n = \delta n_{\max}$ and those in the superluminal region with $\delta n = 0$. The normalized group velocity in the laboratory frame v_g/c is shown for all modes in Fig. 3(a). As the dispersion is normal, the velocity diminishes when the frequency increases.

In the comoving frame, the dimensionless velocity for each mode is given by

$$v'(\omega, \delta n) = \frac{\partial \omega'}{\partial \omega} = n_{g0} \pm \left(\delta n + \frac{2\omega^2 + \Omega_0^2}{\omega^2 + \Omega_0^2} \sqrt{1 + \frac{\omega^2}{\Omega_0^2}} \right). \quad (23)$$

For the counterpropagating and copropagating modes we have

$$v'_u = n_{g0} - \frac{c}{v_g(\omega, \delta n)}, \quad v'_v = n_{g0} + \frac{c}{v_g(\omega, \delta n)}. \quad (24)$$

setting $\delta n = \delta n_{\max}$ for the subluminal region and $\delta n = 0$ for the superluminal. These dimensionless velocities are shown in Fig. 3(b). The copropagating (v) modes are positive for any frequency ω —they move in the same direction as the medium $v(\tau)$ —while the counterpropagating (u) modes invert its direction of travel to low frequencies; the limiting frequencies are the horizons $\pm\omega_h$ and are marked with vertical dashed lines in Fig 3(b). We study next why it is more convenient to define the horizons as frequencies in dispersive systems.

In the sonic case only the counterpropagating curve in the supersonic region 2u inverts its direction of travel [10]. In the optical case both regions 1u and 2u can invert it because the dimensionless velocity fulfills $\delta n \ll n_{g0}$ in both regions close to the horizon for low frequencies. However, for energies close to the horizon—the ones we are interested in—only the 2u modes have low-enough frequencies.

C. Horizons

We have previously defined a horizon as a spatial limit that separates the two regions of spacetime for the modes of the field, as in Fig. 1. We can easily find its location if we match the velocity of the fluctuation with the velocity of the moving medium. In a dispersionless case, as in astrophysics, the horizon is a single spatial point for any frequency of the quantum field. In a dispersive case, as is usual in analog systems, the horizon is fuzzy in space but still uniquely defined in frequency.

For this reason, we define the horizon as the frequency ω_h where the velocity of counterpropagating modes in the superluminal region v'_{2u} is zero, i.e., they are blocked. The definition is then

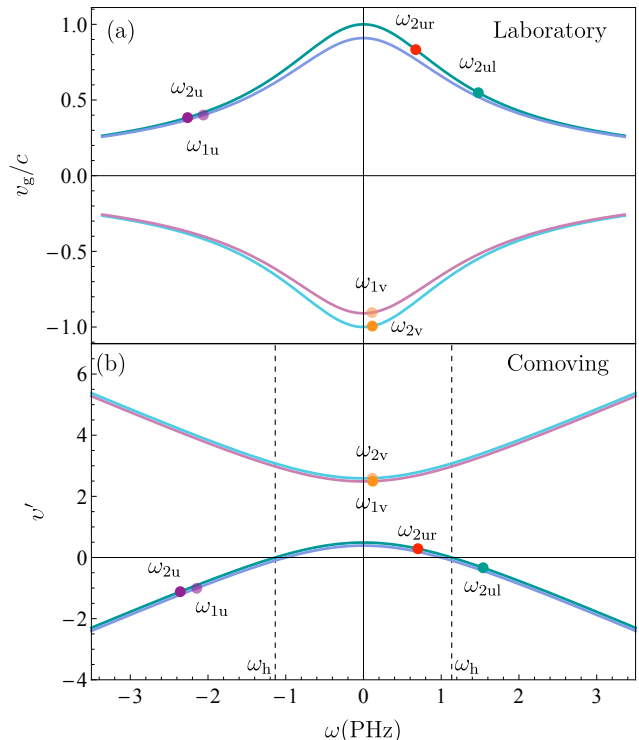


FIG. 3. Group velocity in the laboratory (a) and comoving (b) frames for the 2u (green), 1u (purple), 1v (pink), 2v (blue) modes. The horizons $\pm\omega_h$ are marked with dashed lines and the solutions from Fig. 2 with colored circles.

$$v'_u(\omega)|_{\omega=\omega_h} = 0. \quad (25)$$

Solving this equation, we find

$$\omega_h = \pm \frac{\Omega_0}{2\sqrt{2}} \sqrt{v^2 - 4 \pm v\sqrt{v^2 + 8}}, \quad (26)$$

with $v = v_2$. The general solution for the horizon for any δn is obtained with $v = v'_u$, the counterpropagating velocity in the comoving frame. This equation is equivalent to Eq. (24) in Ref. [29] and Eq. (3.4) in Ref. [10].

D. Transluminal velocity

Now we consider the minimal velocity $v(\tau)$ to reach the horizon, i.e., given ω' , n_{g0} , and Ω_0 , what is the velocity for modes ω_{2ur} and ω_{2ul} to exist (are real) and be equal? We call this the transluminal velocity $v_t = n_{g0} - \delta n_t$ and δn_t the transluminal refractive index. Following Ref. [10], this quantity can be found analytically using an auxiliary function $q(\omega', \Omega_0)$:

$$q = 270 \frac{\Omega_0^2}{\omega'^2} + 729 \frac{\Omega_0^4}{\omega'^4} + \frac{3^{3/2}\Omega_0}{\omega'} \left(27 \frac{\Omega_0^2}{\omega'^2} - 4 \right)^{3/2} - 2, \quad (27)$$

to find

$$\delta n_t = \sqrt{1 + \frac{\omega'^2}{3\Omega_0^2} \left(\frac{q^{1/3}}{2^{1/3}} - 1 \right) + \frac{2^{1/3}}{3q^{1/3}} \left(\frac{\omega'^2}{\Omega_0^2} + 54 \right)}. \quad (28)$$

For example, to fit the infrared horizon in an optical fiber used in analog gravity experiments [13], the values are $\omega' = 0.294\text{PHz}$ and $\Omega_0 = 1.862\text{PHz}$, we find that $\delta n_t = 0.06$. As the value is smaller than $\delta n_{\text{max}} = 0.1$, these frequencies are blocked by the horizons, remain trapped inside the cavity, and are amplified by the Hawking effect; only resonant Hawking radiation escapes the cavity.

IV. INSTABILITIES

Instabilities are inherent to the analysis of the dynamics of fluctuations generated by a moving medium [18]. Up to now we described these fluctuations using its normal modes, i.e., plane waves of the form $e^{-i(\omega\tau + \omega'\zeta)}$, see Eq. (19). These frequencies are usually considered real to describe a plane wave, but in general they can be complex, allowing the introduction of amplification or attenuation processes [19].

We are interested in the process that amplifies Hawking radiation produced as a fluctuation inside the cavity. We take $\omega' = \omega'_R + i\omega'_I$ with $\omega'_I(\omega) > 0$, such that the perturbation grows exponentially with propagation time ζ , such modes are known as unstable. Modes with $\omega'_I < 0$ are known as damped or stable [30] and modes with $\omega'_I = 0$ are called neutral, as those in the previous section. Neutral modes have been used to describe a classical version of the field ϕ in the OBHL and obtain its evolution and amplification [16, 17]. However, in these works the input field needs to be tested one frequency at a time to find those with the highest amplification rate. In this work, we use a quantum description to find the instabilities and obtain the mode with the highest amplification by comparing their respective ω'_I , as this mode dominates the evolution.

A. Analytic method: OBHL with complex frequencies

In this section we apply the theory of instabilities to the OBHL. We first need to generalize the previous solutions to complex values of ω and ω' . Notice that Eq. (18) is a quartic equation in ω and its canonical form is

$$\omega^4 + d\omega^3 + e\omega^2 + f\omega + g = 0, \quad (29)$$

with the following coefficients

$$d = 0, \quad e = (1 - v^2)\Omega_0^2, \quad f = 2v\omega'\Omega_0^2, \quad g = -\omega'^2\Omega_0^2. \quad (30)$$

This type of equations with $d = 0$ can be reduced to an auxiliary cubic equation

$$\omega^3 + \frac{e}{2}\omega^2 + \frac{e^2 - 4g}{16}\omega - \frac{f^2}{64} = 0. \quad (31)$$

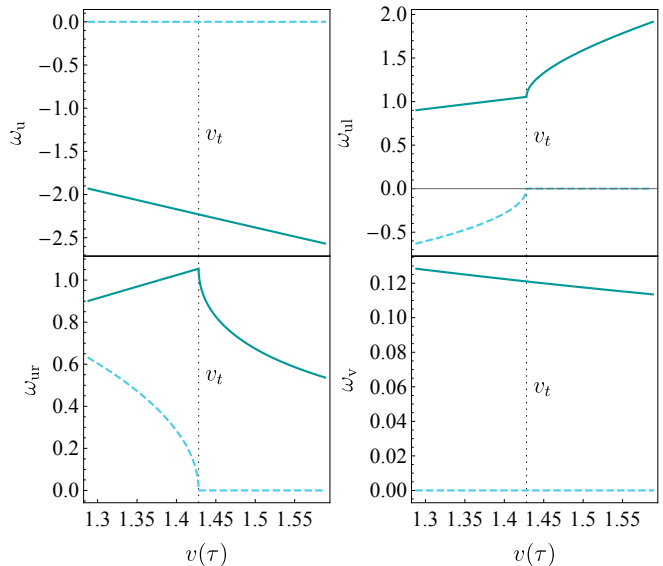


FIG. 4. The four analytic solutions—real (green solid) and imaginary parts (blue dashed)—in terms of the fluid velocity v for fixed values of $\omega' = 0.294\text{PHz}$ and $\Omega_0 = 1.861\text{PHz}$. The transluminal velocity v_t (vertical dashed) is also shown. The solutions ω_u and ω_v are real for any v , but ω_{ur} and ω_{ul} are complex for $v < v_t$.

Its solutions p_1 , p_2 and p_3 can be obtained in the usual way and from those, the four solutions of the quartic equation can be recovered

$$\omega = \sqrt{p_1} \pm (\sqrt{p_2} + \sqrt{p_3}), \quad (32a)$$

$$\omega = -\sqrt{p_1} \pm (\sqrt{p_2} - \sqrt{p_3}). \quad (32b)$$

These are the analytic solutions for the dispersion relation (18); they are very long, but can be used for analytic calculations in symbolic software. In this way, we obtain all four solutions in each region of the OBHL. The behavior of the four complex solutions depends on the value of $v(\tau)$, as seen in Fig. 4. The transluminal velocity v_t marks a change of behavior in the nature of the solutions, where ω_{ur} and ω_{ul} become complex.

Let us return to the solutions analyzed in Section III and shown in Figs. 2 and 3. The analytic solutions for the same conditions are obtained in the complex ω plane and shown as points with black outline in Fig. 5. We obtain the same six results from the numerical method: four in the superluminal region and two in the subluminal region, but also two extra solutions in the subluminal region that are complex conjugate of each other and do not appear in the usual treatment of the OBHL. In Refs. [29, 31] they are called evanescent modes, but they are less relevant as their norm is zero in those treatments. Recently, Isoard and Pavloff [32] used them to calculate the temperature of the Hawking spectrum in a recent experiment in BECs [11]. These additional solutions describe exponentially growing or decreasing modes, and

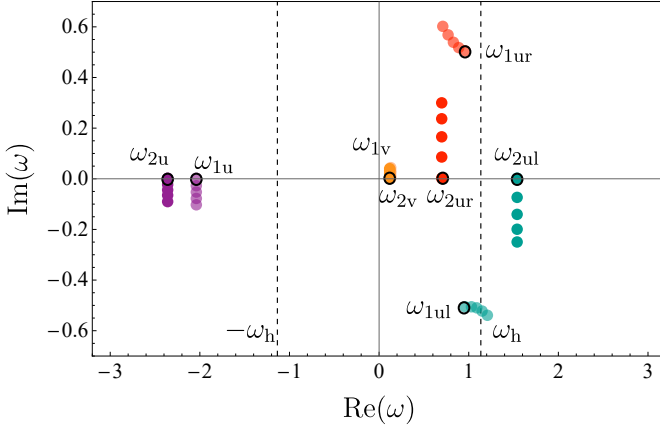


FIG. 5. Analytic solutions in the complex space of ω after adding a small imaginary part $\omega'_I \geq 0$ to ω' . These are the same six real solutions plus two new ones, completing four solutions for both regions. The solutions for $\omega'_I = 0$ are marked with black outline. Dashed lines in ω_h help us find the direction of travel for the 2u modes: ω_{2u} , ω_{2ur} , and ω_{2ul} .

we can write them as

$$e^{-i\omega\tau} = e^{-i(\omega_R+i\omega_I)\tau} = e^{\omega_I\tau} e^{-i\omega_R\tau}. \quad (33)$$

B. Qualitative and quantitative description

We now search for the instabilities of the OBHL; modes with complex comoving frequency $\omega' = \omega'_R + i\omega'_I$ such that $\omega'_I > 0$, whose amplitude increases exponentially with propagation time

$$e^{-i\omega'\zeta} = e^{-i(\omega'_R+i\omega'_I)\zeta} = e^{\omega'_I\zeta} e^{-i\omega'_R\zeta}. \quad (34)$$

We start by finding the conditions that the field fluctuation $\phi(\tau)$ from Eq. (19) must satisfy in τ by dividing it in three regions I, II and III as:

$$\phi_I = \mathbf{A} \cdot e^{-i\omega_1\tau}, \quad \mathbf{A} = (A_1, A_2, A_3, A_4), \quad (35a)$$

$$\phi_{II} = \mathbf{B} \cdot e^{-i\omega_2\tau}, \quad \mathbf{B} = (B_1, B_2, B_3, B_4), \quad (35b)$$

$$\phi_{III} = \mathbf{C} \cdot e^{-i\omega_1\tau}, \quad \mathbf{C} = (C_1, C_2, C_3, C_4), \quad (35c)$$

where

$$e^{-i\omega_1\tau} = (e^{-i\omega_{11}\tau}, e^{-i\omega_{12}\tau}, e^{-i\omega_{13}\tau}, e^{-i\omega_{14}\tau}), \quad (36a)$$

$$e^{-i\omega_2\tau} = (e^{-i\omega_{21}\tau}, e^{-i\omega_{22}\tau}, e^{-i\omega_{23}\tau}, e^{-i\omega_{24}\tau}). \quad (36b)$$

A global mode of the cavity depends on ω' (this fixes four values ω_1 in the subluminal region and other four ω_2 in the superluminal one) and the three vectors \mathbf{A} , \mathbf{B} , \mathbf{C} that describe the mode amplitudes, four complex coefficients in each one.

We consider only normalizable cavity states. For this, we keep only the modes that decay far away from the cavity by setting to zero the amplitude of the unbounded

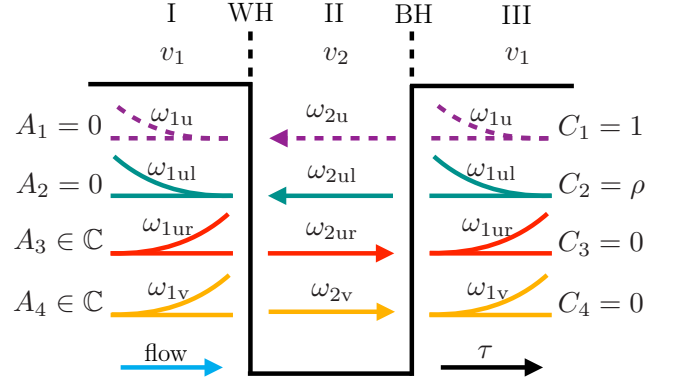


FIG. 6. Mode diagram for an OBHL with instabilities in τ . The coefficients A_j, C_j shown describe the most general normalizable solution for the field ϕ . Solid [dashed] lines refer to positive- [negative-] frequency modes.

modes outside the cavity. From the values in Fig. 5, and the Eq. (33) we notice that $\text{Im}(\omega_{1ur}) > 0$, so it decays to the left $\tau \rightarrow -\infty$, while $\text{Im}(\omega_{1ul}) < 0$ and it decays to the right $\tau \rightarrow \infty$. When we add a small imaginary part $\omega'_I > 0$ to ω' , all ω values become complex points in Fig. 5). Modes with $\text{Im}(\omega) > 0$ increase with τ and modes with $\text{Im}(\omega) < 0$ decrease with it. This behavior is depicted in Fig. 6, where $A_1 = A_2 = C_3 = C_4 = 0$ for the fluctuation $\phi(\tau)$ to be square-integrable. The remaining 8 coefficients should be found to completely describe a cavity mode.

C. Confined states

We use the transfer matrix method to solve this problem [10]. We can use this method under the step-index approximation because the velocity profile is constant everywhere, except at the interfaces, where the solution can be found by the continuity of the quantum field $\phi(\tau)$ and its first three derivatives there. To define the transfer matrices M_1 from region I to II and M_2 from region II to III, we use auxiliary matrices m_1 and m_2 , whose entries are the four amplitudes of the field and its derivatives $(\phi, \phi', \phi'', \phi''')$, i.e.,

$$m_1 = \begin{pmatrix} 1 & 1 & 1 & 1 \\ -i\omega_{11} & -i\omega_{12} & -i\omega_{13} & -i\omega_{14} \\ -\omega_{11}^2 & -\omega_{12}^2 & -\omega_{13}^2 & -\omega_{14}^2 \\ i\omega_{11}^3 & i\omega_{12}^3 & i\omega_{13}^3 & i\omega_{14}^3 \end{pmatrix}, \quad (37)$$

$$m_2 = \begin{pmatrix} 1 & 1 & 1 & 1 \\ -i\omega_{21} & -i\omega_{22} & -i\omega_{23} & -i\omega_{24} \\ -\omega_{21}^2 & -\omega_{22}^2 & -\omega_{23}^2 & -\omega_{24}^2 \\ i\omega_{21}^3 & i\omega_{22}^3 & i\omega_{23}^3 & i\omega_{24}^3 \end{pmatrix}. \quad (38)$$

The first subindex i in ω_{ij} corresponds to the velocity v_1 or v_2 , and the second one j to the particular solution 1-4 ordered always as u, ul, ur, and v—the same order

as in Fig. 6. Then, the transfer matrices are simply

$$M_1 = m_2^{-1}m_1, \quad M_2 = m_1^{-1}m_2 = M_1^{-1}. \quad (39)$$

It is also convenient to define matrices that propagate the solution between the two interfaces of the cavity. These are

$$P_L = \text{diag}(e^{i\omega_{21}\tau_c}, e^{i\omega_{22}\tau_c}, e^{i\omega_{23}\tau_c}, e^{i\omega_{24}\tau_c}), \quad (40)$$

$$P_R = \text{diag}(e^{-i\omega_{21}\tau_c}, e^{-i\omega_{22}\tau_c}, e^{-i\omega_{23}\tau_c}, e^{-i\omega_{24}\tau_c}). \quad (41)$$

Finally, the transfer matrix M from region III to I is

$$M = M_1 P_L M_2 = m_2^{-1}m_1 P_L m_1^{-1}m_2. \quad (42)$$

With M we can obtain the coefficients \mathbf{A} in terms of \mathbf{C} from

$$\phi_I = M\phi_{\text{III}}. \quad (43)$$

In a similar way, we can obtain \mathbf{C} in terms of \mathbf{A} using M^{-1} .

Let us write down the problem: starting from a given comoving frequency ω' and four coefficients \mathbf{C} [\mathbf{A}], we can determine the eight complex frequencies $\omega_1(\omega')$ and $\omega_2(\omega')$ and the other eight coefficients \mathbf{A} and \mathbf{B} [\mathbf{B} and \mathbf{C}].

With the conditions in Fig. 6, we define a spontaneous lasing mode for the OBHL as a mode where the fluctuation $\phi(\tau)$ is square-integrable and the imaginary part of its comoving frequency ω' is positive. The solution for the first coefficient can be found analytically, but the equation for the second one is transcendental and needs to be solved numerically. We can find the instabilities or lasing modes ω'_ℓ varying the two parameters that describe the cavity: the pulse separation τ_c —like “length”—and the optical contrast δn_{max} —like “height”. In Table I we show the number of instabilities N_{ins} found for cavities with parameters $\tau_c = \{6, 13, 20\}$ fs and $\delta n_{\text{max}} = \{0.01, 0.05\}$.

We also calculated the probability of confinement P_c that specifies how much of the probability distribution of the quantum field ϕ is inside the cavity:

$$P_c = \int_0^{\tau_c} d\tau |\phi(\tau)|^2, \quad (44)$$

where $|\phi|^2$ is normalized from $-\infty$ to ∞ . In Fig. 7 we show the probability density $|\phi|^2$ for the instabilities in Table I.

In all solutions found, $P_c < 1$ because there is a possibility that the field tunnels out and escapes the cavity formed by the horizons. This is the typical behavior of resonant Hawking radiation and is similar to the findings in the acoustic system [10, 33, 34]. From Table I and Fig. 7, we see that the ground state increases its confinement with the size of the cavity, i.e., increasing τ_c or δn_{max} .

In this way, we found a discrete set of instabilities ω'_ℓ for a given geometry of the cavity τ_c and δn_{max} . The corresponding values of P_c are also in Table I and the

τ_c (fs)	δn_{max}	N_{ins}	ω'_ℓ (PHz)	P_c (%)	x_a (m)
6	0.01	1	$0.351 + i1.64 \cdot 10^{-6}$	36	9.23
	0.05	1	$0.333 + i6.12 \cdot 10^{-5}$	47	0.25
13	0.01	1	$0.355 + i9.60 \cdot 10^{-7}$	74	1.32
	0.05	2	$0.350 + i1.45 \cdot 10^{-5}$	95	0.09
$0.319 + i4.87 \cdot 10^{-5}$			36	0.31	
20	0.01	2	$0.356 + i4.78 \cdot 10^{-7}$	87	2.58
			$0.349 + i5.08 \cdot 10^{-7}$	21	2.52
	0.05	3	$0.354 + i5.02 \cdot 10^{-6}$	96	0.26
			$0.337 + i2.58 \cdot 10^{-5}$	11	0.06
			$0.312 + i1.16 \cdot 10^{-5}$	60	0.12

TABLE I. Parameters of instabilities in six different cavities with τ_c and δn_{max} .

probability density $|\phi|^2$ in Fig. 7. The number of instabilities N_{ins} increases with τ_c and with δn_{max} in those examples. Is it possible to know before hand how many instabilities are there given the parameters of the cavity? In the next section we compare the solutions found by the theory of instabilities with the resonances of the plane-wave model used in Section III and show that it is possible.

V. INSTABILITIES VS PLANE-WAVE RESONANCES

In the previous section, we showed how to find the instabilities (lasing modes) of an OBHL for any geometry of the cavity ($\tau_c, \delta n_{\text{max}}$). We use now a simple model to get a better physical picture of the lasing modes $\omega(\omega'_\ell)$ with complex frequency $\omega'_\ell = \omega'_R + i\omega'_I$, but now in the limit $\omega'_I \rightarrow 0$, i.e., a plane-wave model with real frequency $\omega(\omega'_R)$ used in Section III.

The modes trapped in the cavity are $\omega_{2\text{ur}}$ and $\omega_{2\text{ul}}$, according to Section III B. Each time one of these modes reaches an horizon, it is amplified through the analog Hawking effect. This evolution still conserves the norm due to the existence of negative-norm modes (dashed lines in Fig 2). After each cycle, a mode $\omega_{1\text{u}}$ leaves the cavity and its amplitude increases with each cycle. This is the so-called plane-wave model and it can verify if the solutions of ω fulfill a cycle condition for the resonance condition [17, 27].

A. Resonance condition

A resonance is produced when trapped radiation has a phase difference of a multiple of 2π after an oscillation period [10, 27]. However, we must also consider the two reflections in each period, one for each horizon and each one producing a phase change of $\pi/2$. Then, the phase difference of trapped modes $\omega_{2\text{ul}}$ and $\omega_{2\text{ur}}$ should fulfill

$$\tau_c \Delta\omega = (2n + 1)\pi, \quad n = 0, 1, 2, \dots \quad (45)$$

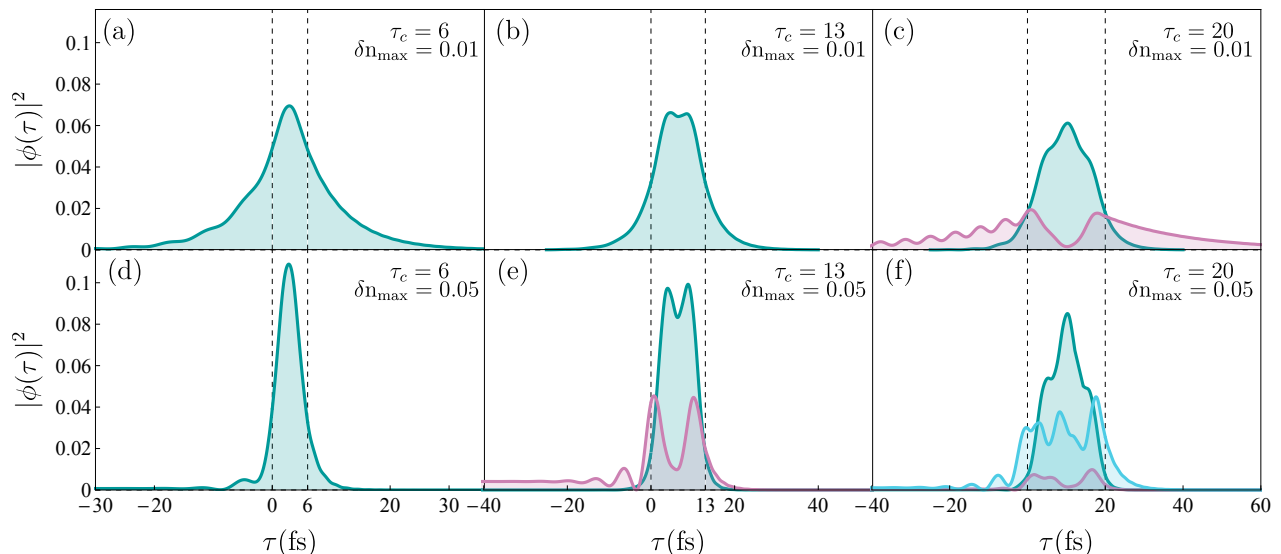


FIG. 7. Probability density $|\phi(\tau)|^2$ of the instabilities for the cavities in Table I. In these examples, the ground state (green) always exists, the first excited state (pink) in three cases, and the second excited state (blue) in one. The vertical dashed lines mark the cavity.

The first resonance ($n = 0$) at $\tau_c \Delta\omega = \pi$ is the ground state instability. The second resonance ($n = 1$) is the first excited state instability and so on.

We can analyze the resonance condition from two points of view: vary τ_c while keeping δn_{\max} fixed and keep τ_c fixed while varying δn_{\max} . Both solutions are shown in Fig. 8, the black points are the resonances resulting from the phase-matching condition in Eq. (45) shown as color curves. The colored points are the instabilities obtained in Section IV for $\tau_c = \{6, 13, 20\}$ fs and $\delta n_{\max} = 0.05$ in (a) and $\tau_c = \{6, 13\}$ fs and $\delta n_{\max} = \{0.01, 0.05\}$ in (b).

In most cases, the frequencies ω'_R predicted for the resonances are close to those for the instabilities, their values differ less than 7%. Their discrepancy can be explained because the resonance condition (45) does not contain information about the “height” of the cavity δn_{\max} . The only information imposed for resonances is the minimum value δn_{\max} to trap the mode ω'_R , given by the condition $\delta n_{\max} > \delta n_t$, as shown in Fig. 8(b).

The number of resonances in the plane-wave model in the parameter space of the cavity geometry $(\tau_c, \delta n_{\max})$ is shown in Fig. 9. The colored regions limited by solid black lines show the parameters for the number of resonances from 0 to 4. We can compare it with the number of instabilities N_{ins} found for several cases including those from Table I and Fig. 7. The resonances approximate the number of solutions but they do not capture all the physics, e.g., there are several geometries in Fig. 9 where there is one more instability than resonances. This is expected as there is slightly more flexibility for an instability to be square-integrable because its parameters are complex $\omega' \in \mathbb{C}$, these cases are the ones where the difference in frequency is larger.

B. Phenomenological model

We introduce a phenomenological model to characterize the number of instabilities or resonant modes in a cavity. This model is taken directly from fiber optics, where it is used to calculate the number of modes allowed in a fiber [35]. The cavity in this case is the physical transversal dimensions of the fiber, usually limited by a core. This model is described by the parameter V , given by

$$V = k_0 a \sqrt{n_1^2 - n_2^2}, \quad (46)$$

where k_0 is the wavenumber of the radiation, a is the core radius, n_1 and n_2 are the two index of refraction that make the optical contrast. Making the changes of variables to match our geometry, where the radiation is trapped not in the transversal dimension as in a fiber, but in the longitudinal direction or delay, the equation would be

$$V_\tau = \left(\frac{\omega'(\omega_h)}{2} \right)^2 \tau_c^2 \delta n_{\max}. \quad (47)$$

The parameter V_τ is dimensionless and depends on the geometry and contrast of the longitudinal cavity. The values of V_τ are limited by red dashed lines in Fig. 9, where it is clear that this phenomenological model matches very well to the number of resonances. This shows a simpler way to predict the number of resonant modes for a given geometry of the cavity. For example, for $V_\tau < 0.028$ there are no resonances and for $0.028 < V_\tau < 0.253$ there is a single resonance. This is similar to the way that parameters of single-mode fibers are found in the original use of the phenomenological model with V .

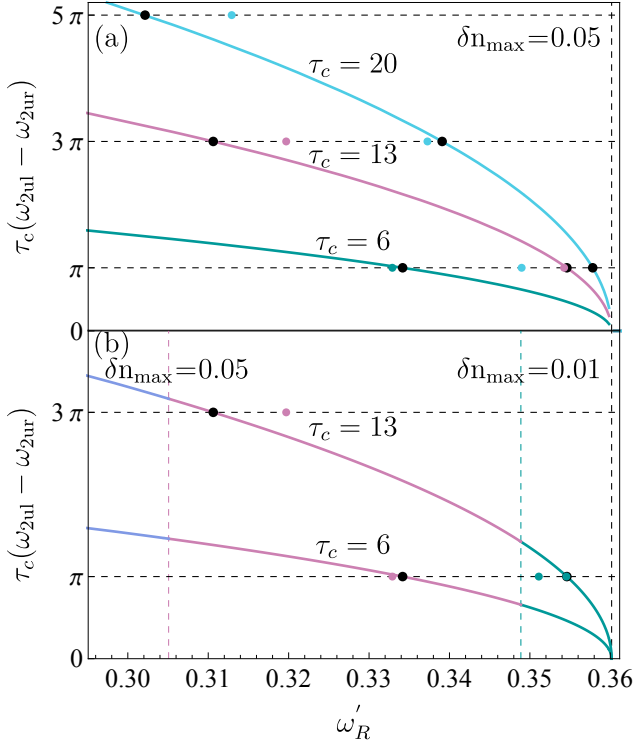


FIG. 8. (a) Phase difference $\tau_c \Delta\omega$ for varying τ_c and fixed δn_{\max} . The phase differences for π , 3π and 5π for the resonances are marked with black points and the instabilities with colored points. (b) Fixed τ_c and varying δn_{\max} , marked with vertical dashed lines. Resonances should be on the right side of these lines.

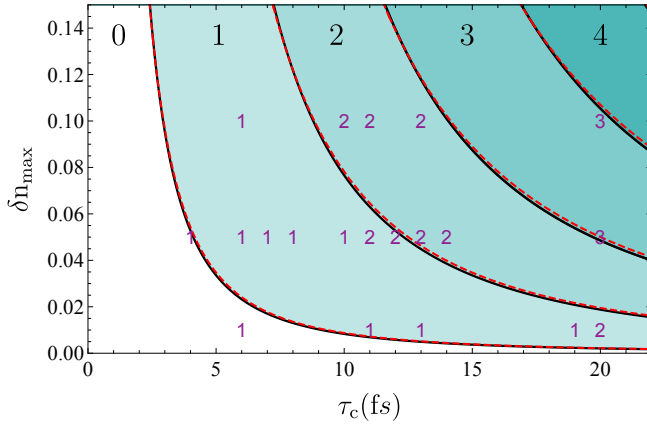


FIG. 9. Number of resonances in the parameter space of the geometry of the cavity $(\tau_c, \delta n_{\max})$. The colored regions have 0 to 4 resonances (large black numbers) separated by a black line. The number of instabilities N_{ins} (small purple numbers) in the corresponding point of the parameter space goes from 1 to 3. The red dashed lines come from the phenomenological model for instabilities in Eq. (47), it matches well the resonances.

C. Propagation time

Up to now, we have verified that the cavity modes are square integrable in the delay τ and that ω'_R , the real part of ω'_ℓ , fulfills the resonance condition; now we want to focus on the information given by its imaginary part ω'_I . According to Eq. (34), this quantity describes the amplification rate of the instability in terms of the propagation time ζ . In a cavity with more than one instability, the one with larger ω'_I is amplified faster and quickly dominates over other instabilities.

We can set numerical values and calculate the propagation time by considering that the model stops working when the energy of the quantum fluctuation is the same as the energy of the classical cavity that holds it, this is our figure of merit. In fact, the energy of the fluctuations is taken from the cavity, as in the Hawking process the energy for the photon production is taken from whatever causes the curvature or surface gravity. In the astrophysical case this is the mass of the black hole, and in optical analogs is the light pulses causing the optical contrast δn of the cavity. This means that the model stops working before this point, but this gives us the order of magnitude of the corresponding amplification time ζ_a and distance x_a .

Due to energy conservation, the total energy density in the system ρ_S must be the same at any time ζ . Then

$$\rho_S(0) = \rho_\ell(\zeta) + \rho_c(\zeta), \quad (48)$$

where ρ_ℓ is the part of the instability

$$\rho_\ell(\zeta) = \hbar\omega_\ell |\phi_{\max}|^2 e^{2\omega'_I \zeta}, \quad (49)$$

and ω_ℓ belongs to the instability that maximizes $|\phi_{\max}|^2$ inside the cavity. The term ρ_c is the energetic part of the cavity formed by light pulses

$$\rho_c(\zeta) = \rho_c(0) e^{-2\omega'_I \zeta}, \quad (50)$$

where $\rho_c(0)$ is the initial energy density of the cavity that gives energy to the fluctuation. To find it, recall from Eq. (20) that δn_{\max} is related to the maximum intensity of the pulse by $I = \delta n_{\max}/n_2$, then

$$\rho_c(0) = \frac{\delta n_{\max} A}{n_2}, \quad (51)$$

where n_2 is the nonlinear index and A is the effective mode area of the fiber. Replacing Eq. (51) in Eqs. (49) and (50) and after some algebra we find

$$\zeta_a = \frac{1}{2\omega'_I} \ln \left(\frac{\delta n_{\max} A}{\hbar\omega_\ell |\phi_{\max}|^2 n_2} \right), \quad (52)$$

this is the lifetime of the instabilities. The distance traveled by the mode inside the optical fiber in that time is $x_a = u\zeta_a$. A photonic-crystal fiber commonly used in analog Hawking radiation experiments has nonlinear index $n_2 = 2.2 \times 10^{-20} \text{m}^2/\text{W}$ [35], effective area

$A = 7.84 \times 10^{-14} \text{m}^2$, and group velocity $u = 0.2014 \mu\text{m}/\text{fs}$ [36]. The amplification distances x_a are reported in the last column in Table I, where the order of magnitude is of meters. This means that the self-amplified Hawking radiation should obtain high levels of energy, comparable to classical ones, while it propagates in a meter-long fiber.

VI. CONCLUSIONS

In this work we found the dispersion relation for a quantum field fluctuation in an optical fiber. A light pulse propagating inside the fiber creates analogs of the event horizon and, under certain conditions, a fluctuation is generated spontaneously in an amplification process similar to that of Hawking radiation in an astrophysical black-hole: This is the optical analog of the Hawking effect.

This fluctuation can be further self-amplified if its generated in a configuration known as optical black-hole laser, where two pulses trap and amplify the radiation using the energy of light that forms the cavity. This configuration is usually described by plane-wave modes with real frequencies.

In this work we allowed all the frequencies to be complex and use the theory of instabilities. We restrict ourselves to solutions whose real part of the comoving frequency is positive to describe amplification processes. With this, we obtained the instabilities as the global cavity modes that are normalizable. The instabilities are trapped inside the cavity and their probability distribution behaves as that of eigenstates in quantum mechanics, e.g., the increasing number of maxima in the unstable

modes shown in Fig. 7 and the fact that the confinement increases for a larger cavity.

We compared our results for the instabilities by comparing with the resonant conditions in the plane-wave model. We found a good agreement considering that the plane-wave model has some limitations. We described the evolution of self-amplifying radiation inside the cavity that is usually hidden in more complicated models [16, 17]. For example, the fact that analog Hawking radiation can tunnel out of the cavity, similar to the usual behavior of Hawking radiation.

We also used a phenomenological model inspired by fiber optics to predict the number of resonances and instabilities. This models matches almost perfectly with the number of resonances and can be obtained simply with the length and optical contrast of the cavity and the frequency of the initial Hawking radiation. Lastly, with a simple model we obtained the order of magnitude of lifetime of the instabilities.

A deeper understanding of the parameter region where the number of instabilities and resonances do not match is needed. It would be also interesting to design a cavity with the highest amplification rate of Hawking radiation. One thing is certain, the theory of instabilities is a powerful tool that can be used in the study of resonant Hawking radiation.

ACKNOWLEDGMENTS

JRE would like to acknowledge the financial support of Conacyt (Mexico) through scholarship 637736. The authors acknowledge the financial support of Secretaría de Educación Pública (Mexico) and Centro de Investigación y de Estudios Avanzados, project 60-2018.

-
- [1] S. W. Hawking, *Nature* **248**, 30 (1974).
 - [2] A. D. Helfer, *Reports on Progress in Physics* **66**, 943 (2003).
 - [3] M. Visser, *International Journal of Modern Physics A* **12**, 649 (2003).
 - [4] W. G. Unruh, *Physical Review Letters* **46**, 1351 (1981).
 - [5] S. Weinfurtner, E. W. Tedford, M. C. J. Penrice, W. G. Unruh, and G. A. Lawrence, *Physical Review Letters* **106**, 021302 (2011).
 - [6] L.-P. Euvé, F. Michel, R. Parentani, T. G. Philbin, and G. Rousseaux, *Physical Review Letters* **117**, 121301 (2016).
 - [7] G. E. Volovik, *The universe in a helium droplet*, Vol. 117 (Oxford University Press on Demand, Oxford, 2003).
 - [8] T. A. Jacobson and G. E. Volovik, *Physical Review D* **58**, 064021 (1998).
 - [9] I. Zapata, M. Albert, R. Parentani, and F. Sols, *New Journal of Physics* **13**, 063048 (2011).
 - [10] D. Bermudez and U. Leonhardt, *Classical and Quantum Gravity* **36**, 024001 (2018).
 - [11] J. R. M. de Nova, K. Golubkov, V. I. Kolobov, and J. Steinhauer, *Nature* **569**, 688 (2019).
 - [12] T. G. Philbin, C. Kuklewicz, S. Robertson, S. Hill, F. König, and U. Leonhardt, *Science* **319**, 1367 (2008).
 - [13] J. Drori, Y. Rosenberg, D. Bermudez, Y. Silberberg, and U. Leonhardt, *Physical Review Letters* **122**, 010404 (2019).
 - [14] G. Jannes, P. Maïssa, T. G. Philbin, and G. Rousseaux, *Physical Review D* **83**, 104028 (2011).
 - [15] S. Corley and T. Jacobson, *Physical Review D* **59**, 124011 (1999).
 - [16] D. Faccio, T. Arane, M. Lamperti, and U. Leonhardt, *Classical and Quantum Gravity* **29**, 224009 (2012).
 - [17] J. L. Gaona-Reyes and D. Bermudez, *Annals of Physics* **380**, 41 (2017).
 - [18] U. Leonhardt, T. Kiss, and P. Öhberg, *Physical Review A* **67**, 033602 (2003).
 - [19] F. Charru, *Hydrodynamic Instabilities*, Cambridge Texts in Applied Mathematics 37 (Cambridge University Press, 2011).
 - [20] P. D. Drummond, *Physical Review A* **42**, 6845 (1990).
 - [21] P. D. Drummond and M. Hillery,

- The quantum theory of nonlinear optics (Cambridge University Press, 2014).
- [22] S. Robertson, *Journal of Physics B: Atomic, Molecular and Optical Physics* **45**, 163001 (2012).
- [23] D. Bermudez and U. Leonhardt, *Physical Review A* **93**, 053820 (2016).
- [24] M. J. Jacquet and F. Koenig, *arXiv preprint 1908.02060 [quant-ph]* (2019).
- [25] B. W. Plansinis, W. R. Donaldson, and G. P. Agrawal, *Journal of the Optical Society of America B* **33**, 1112 (2016).
- [26] M. Jacquet and F. König, *Physical Review A* **92**, 023851 (2015).
- [27] U. Leonhardt and T. G. Philbin, *Lect. Notes Phys.* **718**, 229 (2007).
- [28] S. Robertson, Hawking radiation in dispersive media, Ph.D. thesis, St. Andrews, St. Andrews (2011).
- [29] P.-É. Larré, A. Recati, I. Carusotto, and N. Pavloff, *Physical Review A* **85**, 013621 (2012).
- [30] F. Gallaire and P.-T. Brun, *Philosophical Transactions of the Royal Society A: Mathematical, Physical and Engineering Sciences* **375**, 20160155 (2017).
- [31] M. Isoard, Fluctuations quantiques en gravité analogue, Master's thesis, Laboratoire de Physique Théorique et Modèles Statistiques (2017).
- [32] M. Isoard and N. Pavloff, *Physical Review Letters* **124**, 060401 (2020).
- [33] J. Curtis, G. Refael, and V. Galitski, *Annals of Physics* **407**, 148 (2019).
- [34] A. Coutant, Y. Aurégan, and V. Pagneux, *The Journal of the Acoustical Society of America* **146**, 2632 (2019).
- [35] G. P. Agrawal, Nonlinear fiber optics, 5th ed. (Academic Press, New York, 2013).
- [36] D. Bermudez, *Journal of Physics: Conference Series* **698**, 012017 (2016).